ELSEVIER

Ceramics International 25 (1999) 215–222

CERAMICS INTERNATIONAL

Upgrading superplastic deformation performance of fine-grained alumina by graphite particles

A. Bataille *, J. Crampon, R. Duclos

Laboratoire de Structure et Propriétes de l'Etat Solide, URA-CNRS 234, Bât. C6 - Cité Scientifique, Université des Sciences et Technologies de Lille, 59 655 Villeneuve D'Ascq, Cedex, France

Received 19 December 1997; accepted 27 February 1998

Abstract

The process of ceramic part forming is often accompanied by grain growth, which in turn limits the deformation capabilities. Alumina ceramics are not usually good candidates for superplasticity as the grain growth reduces quickly their deformation performance. In order to impede the grain boundary mobility and to limit the grain growth, zirconia has often been associated with the alumina since the early 80s. In this work, a dense MgO-doped α-alumina containing a small amount of carbon has been produced. The sintering and the deformation behaviour of this material are compared to those of a MgO-doped alumina. The presence of small carbon particles reduces greatly the grain growth during the sintering and during the compression experiments. The superplasticity of the carbon-containing alumina is greatly improved.

1. Introduction

A growing range of structural ceramics have presented interesting performances in terms of superplastic deformation [1–5]. However these ceramics require a submicrometer grain size and a high temperature to exhibit a superplastic behaviour [5–9]. The thermal stability of such a grain size is a critical issue and its control is thus an essential step in achieving applicable superplasticity for structural ceramics.

Static and dynamic changes in grain size during deformation contribute to the overall growth which usually reduces continuously the superplastic capacity of the considered material. Different approaches have been experimented in order to control the grain growth during the deformation: (1) MgO has been added to alumina in order to lower the grain boundary mobility through solute drag [3] and (2) ZrO_2 particles have been particularly useful in impeding the grain growth of alumina by second phase pinning [2,3,7]. However the MgO effect is limited and one problem arises with the addition of ZrO_2 particles: their effectiveness is related to the homogeneity of their distribution which can evolve during the deformation of the material.

In the present work, another route was utilized for controlling the grain growth: a MgO-doped α-alumina polycrystal with a homogeneous distribution of graphite-pinning particles was produced. Those particles resulted from the thermal decomposition, during hot-pressing under vacuum, of the polymers used for the atomization of the alumina powder. In order to characterize the effect of those carbon particles, the hot-pressing procedure was also carried out on the calcined MgO-doped α-alumina powder. The microstructure investigations of the two sets of materials are presented and compared to each other. Moreover the compressive deformation behaviour of both materials are examined and compared at $T = 1400°C$ in air and under vacuum. The presence of carbon in the form of precipitates results in a remarkable improvement of superplastic behaviour of the α-alumina. Compressive deformations of true strains up to $\varepsilon = -0.7$ were achieved at a strain rate $\dot{\varepsilon} = 10^{-4}\ s^{-1}$ at $T = 1400°C$ at low flow stresses (less than $\sigma = 40$ MPa) with only limited density loss. The correlations between strain rates, stresses and grain sizes are discussed in relation to different deformation mechanisms.

* Corresponding author.

0272-8842/99/$—see front matter
PII: S0272-8842(98)00026-1

2. Experimental procedure

The starting material used in the study was an atomized commercial 500 ppm MgO-doped α-alumina powder (Baikowski SM8). The nominal composition of the alumina powder is given in Table 1. In addition the atomization process introduced 1.3 wt.% of carbon.

From this powder two sets of dense alumina materials were produced. The first set was produced directly from the as-received alumina powder (hereafter uncalcined alumina or UA) whereas for the second set, calcination of the powder was conducted before processing to eliminate organic compounds resulting from atomization (hereafter calcined alumina or CA). Discs were first cold-pressed ($\sigma = 20$ MPa) and then hot-pressed ($\sigma = 45$ MPa) during 30 min at $T = 1450$°C in a graphite die, heating rate being 10°C. min^{-1}. Hot-pressing was performed under vacuum (less than 10^{-2} Pa on average) in a graphite heating element furnace. The obtained alumina discs had a diameter of 30 mm and a height of 10 mm.

Density of the resulting billets was determined by weighing in alcohol using the Archimedes' method. Final densities greater than 99.5 % of theoretical were reached for all billets. Samples for deformation experiments were cut from the hot-pressed billets and the faces were made parallel. Typical sample sizes were a transverse square section of 4.5×4.5 mm^2 and a height of 10 mm.

Two kinds of deformation tests were performed:

(i) Compression tests under vacuum were experimented on a universal screw-driven testing machine. The vacuum pressure was less than 10^{-3} Pa on average. The specimen was placed between parallel nuclear grade graphite rods. These rods were attached to the base and to the crosshead of the testing machine. All the tests were done at a constant crosshead displacement rate (60 mm.min^{-1}, corresponding to an initial true deformation rate of $\dot{\varepsilon}_0 = 10^{-4}$ s^{-1}). From load versus time curves, true stress versus true strain curves were calculated.

(ii) Compressive creep tests in air concerning only the CA specimens were carried out at constant true stress (30 MPa). From length change versus time curves, true strain rate versus true strain curves were obtained. The microstructures of as-hot-pressed and of strained specimens were characterized by scanning electron microscopy (SEM) and by conventional transmission electron microscopy (TEM) or high resolution transmission electron microscopy (HRTEM). For SEM investigations, diamond polished cross sections were thermally etched at $T = 1400$°C for 90 min to reveal the microstructure. The grain sizes were obtained by multiplying the square root of the average grain surface by 1.38 [1]. More than three hundred grains were numbered for each grain size calculation.

Table 1
Nominal composition (wt. ppm) of alumina + 500 wt. ppm MgO before atomization

Fe	Na	K	Si	Ca	Cr
10	17	38	38	8	4

3. Results

3.1. Microstructures of hot-pressed materials.

TEM micrographs of hot-pressed UA and CA samples are presented in Fig. 1. At standard magnification (20 k), both micrographs exhibit microstructures similar to those of single phase materials. However the effect of residual carbon is already easily perceptible since the mean grain size is 1.26 μm for the CA specimens

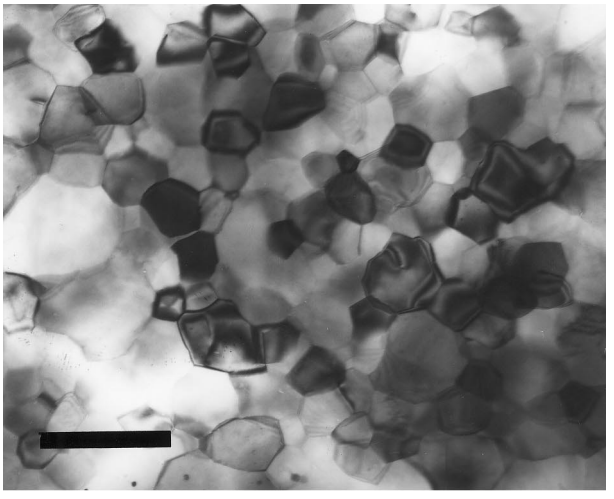

(a)

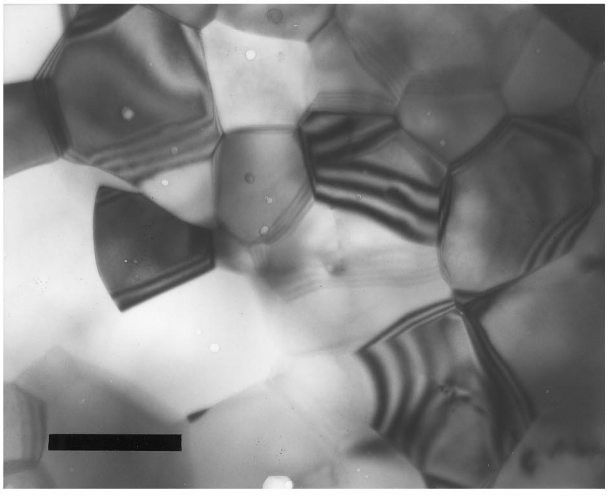

(b)

Fig. 1. Transmission electron micrographs of the as-sintered UA (a) and CA (b) materials. Scale bar: 1 μm.

whereas it is as fine as 0.56 μm for the UA ones. The ratio between the mean grain linear lengths measured in direction respectively parallel to and perpendicular to the pressure axis is the aspect ratio. For both hot-pressed materials, it is about unity. No dislocation were observed in the microstructures of studied materials.

At higher magnification, TEM micrographs of UA specimens account for a homogeneous distribution of graphite particles in the microstructure, the mean distance between two precipitates being in the range 20–40 nm. Fig. 2 illustrates this observation whereas Fig. 3 shows HRTEM micrographs of particles located into a grain or at a grain boundary. According to observations, the individual volume of the platelet-like precipitates was estimated at about $10^3\,nm^3$. In addition, HRTEM observations revealed that some graphite particles presented a slight crystalline contrast which corresponds to the turbostratic form [10].

3.2. Deformation tests.

Fig. 4a shows typical true stress versus true strain curves obtained at $T = 1400°C$ under vacuum at an initial true strain rate $\dot{\varepsilon} = 10^{-4}\ s^{-1}$ for UA and CA materials. These curves exhibit two kinds of behaviour related to the microstructural differences:

1. the initial flow stress of CA material is about twice that of UA one (respectively 35 MPa and 18 MPa in Fig. 4a),
2. the strain hardening is much higher for the CA material than for the UA material. The CA material has been creep-tested at different stresses and temperatures. Fig. 4b presents a typical true strain rate versus true strain curve obtained in air for the CA material creeped at $T = 1400°C$ and under $\sigma = 30$ MPa. There is an important decrease in true strain rate with the true strain.

In terms of true stress and true strain rate, the CA material exhibits the same deformation behaviour regardless to the atmosphere: at true stresses $\sigma = 35$ MPa under vacuum (Fig. 4a) and $\sigma = 30$ MPa in air (Fig. 4b), initial true strain rates are respectively $\dot{\varepsilon}_0 = 10^{-4}\ s^{-1}$ and $\dot{\varepsilon}_0 = 7.10^{-5}\ s^{-1}$ (see Fig. 4b for the latter). We have considered the expression of the constitutive equation of superplastic deformation, i.e.

$$\dot{\varepsilon} = C.\sigma^n.d^{-p}.\exp(-\frac{\Delta H}{RT}) \quad (1)$$

where is $\dot{\varepsilon}$ the true strain rate, σ is the true stress, d is the grain size, n and p are the stress and the grain size exponents respectively and ΔH is the activation energy. The isostructural activation energies and the isostructural stress exponents were respectively determined

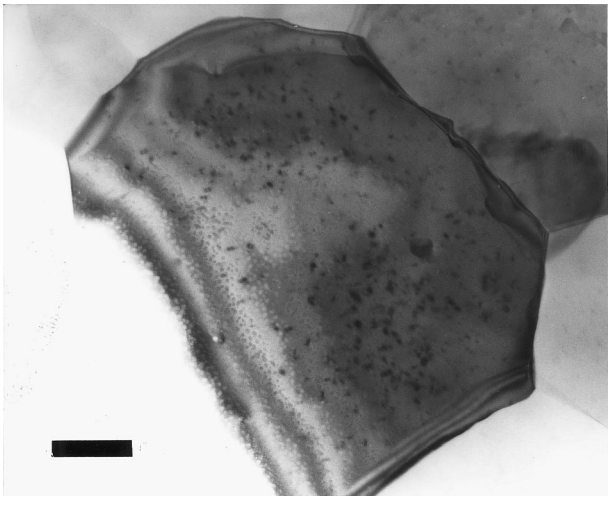

Fig. 2. Transmission electron micrograph showing the homogeneous distribution of the graphite precipitates. Scale bar: 100 nm.

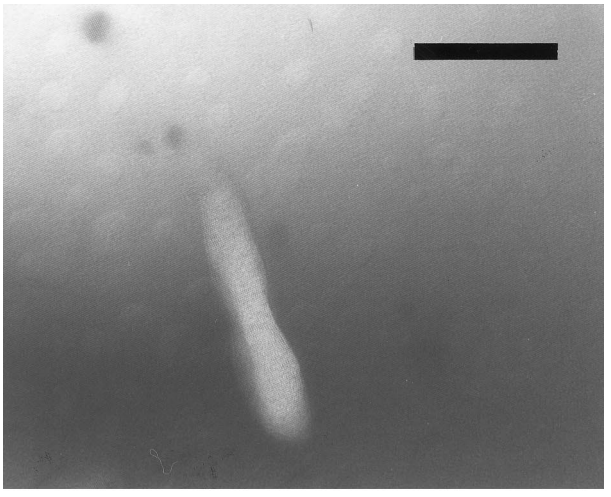

(a)

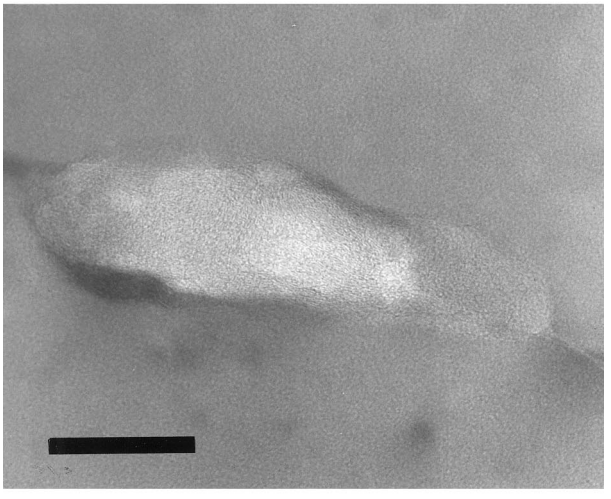

(b)

Fig. 3. HRTEM observations of turbostratic graphite precipitate in the UA grain (a) and at the UA grain boundary (b). Scale bar: 25 nm.

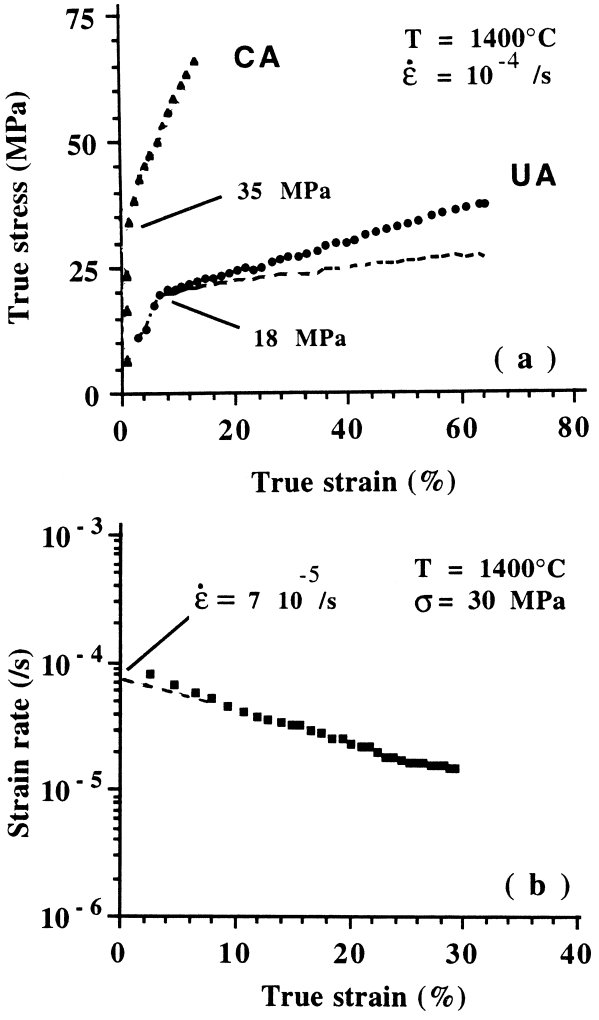

Fig. 4. True stress versus true strain curves under vacuum for both CA and UA materials at $\dot{\varepsilon}_0 = 10^{-4}$ s^{-1} (a) and strain rate versus true strain curve in air for CA at $\sigma = 30$ MPa (b).

at constant stress by a temperature change method or at constant temperature by a stress or a displacement rate change method.

Table 2 summarizes the mean of results obtained for n and ΔH together with the respective scatter. The activation energy values are quite similar for both materials whereas the stress exponents are very different. Moreover, there is no significant difference between results obtained under vacuum or in air for CA material.

3.3. Microstructures of strained materials.

Fig. 5 presents SEM micrographs of the strained specimens. Grain growth is evident for the two materials. At a true strain $\varepsilon = -0.30$, the mean grain size of the CA material is $d = 2.62\,\mu$m when it reaches only $d = 0.81\,\mu$m for UA one. For the CA material the aspect ratio is 0.88 for a true strain of $\varepsilon = -0.30$. The deformation of the UA material at a true strain $\varepsilon = -0.65$ results in a ratio of 0.74. Hence the grain shape do not change in any significant manner during the deformation.

TEM observations of the UA material did not reveal grain boundary damage nor cavitation at a true strain $\varepsilon = -0.65$ (see Fig. 6). From Fig. 5, it is observed that the CA material presents cavitation at grain boundaries and at triple junctions in the compressive deformation. Dislocations were seldom observed in the strained materials.

Table 2
Stress exponent values (n) at $T = 1400$°C and activation energy values (ΔH)

Material atmosphere	UA vacuum	CA vacuum	CA air
n (+/− 0.2)	2.4	1.6	1.24
ΔH (+/− 50 kJ/mol)	515	560	540

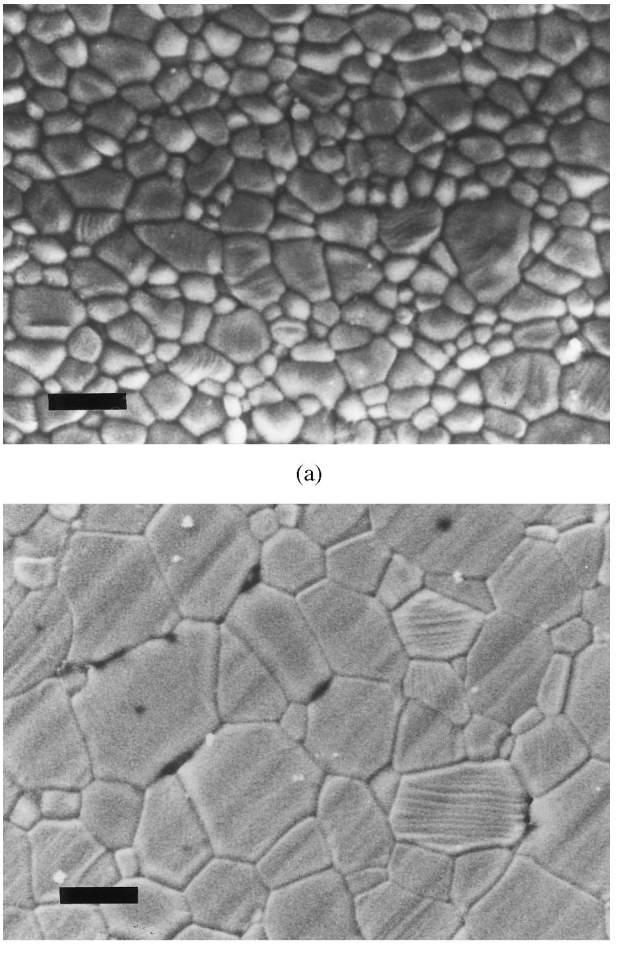

(a)

(b)

Fig. 5. SEM micrographs of strained specimens. $T = 1400$°C and $\dot{\varepsilon}_0 = 10^{-4}$ s^{-1}. UA material for $\varepsilon = -0.65$ (a) and CA material for $\varepsilon = -0.30$ (b). Scale bar: 2 μm.

Sample densities have been measured before and after deformation tests. The related data are listed in Table 3. There is no important density change for the UA material whatever the final strain whereas the results corresponding to the CA material show a slight decrease of the specimen independently of the experiment atmosphere.

4. Discussion

4.1. Strain hardening

Concerning the tests carried out under vacuum, at a constant crosshead displacement rate, the compressive deformation of the specimen entails an increase in the true strain rate and consequently an increase in the true stress. The corrected true stress σ_{cor} that would correspond to a constant true strain rate $\dot{\varepsilon}$ (the initial value of the true strain rate) can be determined from the knowledge of the true strain ε and of the stress exponent n.

Indeed, at any time, the true strain rate can be related to $\dot{\varepsilon}_0$ and to the nominal strain ε_0 by :

$$\dot{\varepsilon} = \frac{\dot{\varepsilon}_0}{1+\varepsilon_0} \tag{2}$$

According to relations (1) and (2), at a constant true strain rate $\dot{\varepsilon}_0$, the corrected true stress would be :

$$\sigma_{cor} = \sigma.\exp\left(\frac{\varepsilon}{n}\right) \tag{3}$$

Note the true compressive strain ε is negative. The broken line in Fig. 4a shows the corrected true stress versus true strain curve at a constant true strain rate $\dot{\varepsilon} = 10^{-1}$ s^{-1} for UA material. There is still a strain hardening for UA. Concerning the CA material data, the correction has not been applied since the corresponding true strain was less than -0.2.

Both SEM and TEM observations have revealed a grain growth during the tests. To account for a possible effect of dynamic grain growth, a mechanism that is well-known to operate during deformation of a range of ceramic materials [1,5,7,11,12], the effect of time only on the grain growth (static grain growth) has been studied at $T = 1400°C$ and the results compared with experimental grain sizes of strained specimens (Fig. 7). Note that the time corresponding to the different deformation tests is less than 90 min under vacuum and it is about 6 h in air. As can be seen in Fig. 7, the grain sizes of the strained specimens are much higher than those resulting from a static grain growth at a corresponding annealing time. Therefore the grain growth is mainly attributed to dynamic grain growth. Wilkinson et al [13] treated the dynamic grain growth and proposed a simple relation between the grain growth per unit strain and the grain size. The general relation between the current value of the grain size d and the negative true strain is:

$$d = d_{ini}.\exp(-B.\varepsilon) \tag{4}$$

where d_{ini} corresponds to the initial grain size. By neglecting the static grain growth in regard to the importance of the dynamic one, the Wilkinson's relation is applied to our case. Fig. 8 presents the experimental data and the fitting curves associated with relation (4). The UA and CA grain growth are quite well described by the two following relations:
for the UA material,

$$d = d_{ini}.\exp(-\varepsilon) \tag{5}$$

for the CA material,

$$d = d_{ini}.\exp(-2.45\varepsilon) \tag{6}$$

Table 3
Relative d/TD versus true strain ε under vacuum and in air at $T = 1400°C$ (TD stands for theoretical density which is 4)

UA material under vacuum			
(ε) d/TD	(0) 99.7 %	(−0.30) 99.5 %	(−0.65) 99.2 %
CA material under vacuum			
(ε) d/TD	(0) 99.9 %	(−0.12) 99.4 %	
CA material in air			
(ε) d/TD	(0) 99.9 %	(−0.30) 99.1 %	(−0.50) 97.8 %

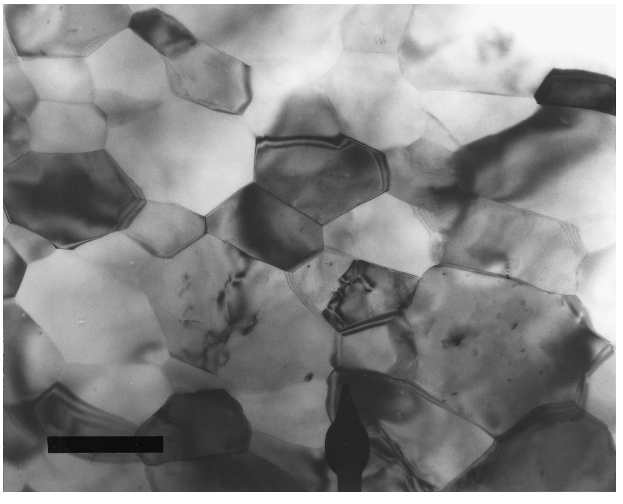

Fig. 6. Transmission electron micrograph of the microstructure of a deformed UA sample at $\varepsilon = -0.65$. $\dot{\varepsilon}_0 = 10^{-4}$ s^{-1}, $T = 1400°C$. Scale bar: 1 μm.

The difference between the B values accounts for the observed variations in the amplitude of grain growth for the considered strains.

4.2. Calculation of p values

To complete the Eq. (1), the values of the grain size exponent p have still to be determinated from the tests under vacuum and in air. First of all we assume that the residual increase of the corrected flow stress during the tests (see Fig. 4a) is only related to the grain growth. Taking into account the grain size change in the constitutive Eq. (1), the true stress σ_{ini} corresponding to the initial grain size d_{ini} and to a constant true strain rate would be :

$$\sigma_{ini} = \sigma_{cor}.\left(\frac{d}{d_{ini}}\right)^{-p/n} \quad (7)$$

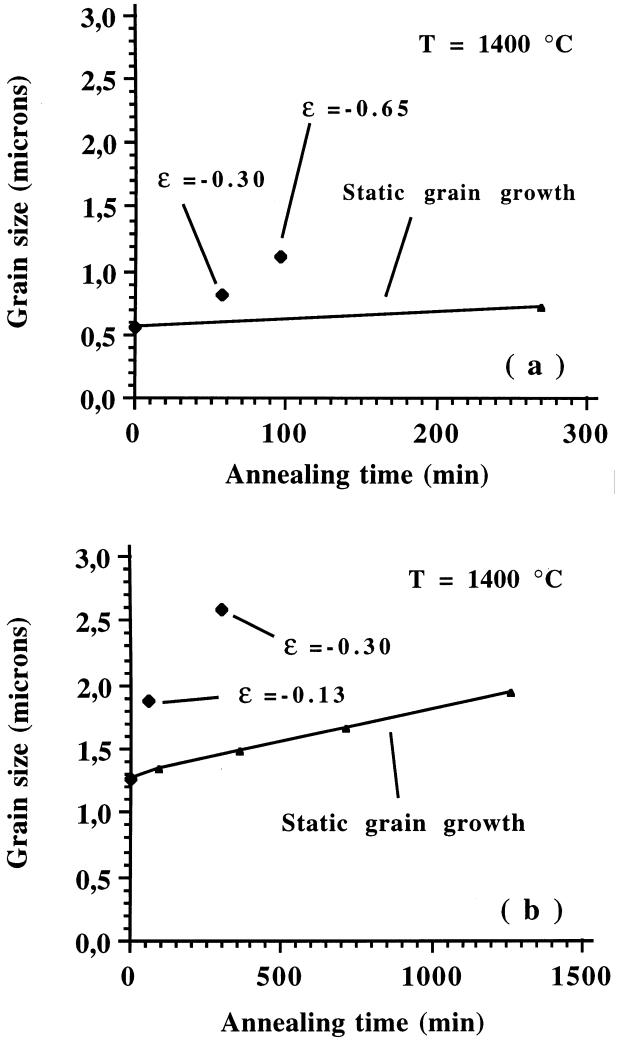

Fig. 7. Time and strain effects on grain growth kinetics for UA (a) and CA (b) at $T = 1400°C$.

The average p values for the tests under vacuum can be drawn from this relation. For the creep tests in air, the true stress is constant and after the transient creep, a constant strain rate decrease is obtained (Fig. 4b). Extrapolating the strain rate variation to $\varepsilon = 0$ gives the value of the strain rate for the initial grain size d_{ini}. The ratio of the current strain rate to the extrapolated initial value equals the ratio of the grain sizes powered to $-p$. The value of p is then calculated and the results are listed in Table 4. The scatter of p values for each determination is about $+/-$ 0.2. For the CA material, the p value seems insensitive to the experiment atmosphere. The p value of the UA material is much lower than that of the CA one, indicating a difference in deformation behaviours.

4.3. Effect of the carbon particle distribution

Now the carbon content of the UA material and the particle distribution must be considered. According to observations of hot-pressed and strained UA specimens, the size and distribution of graphite particles are not affected by deformation and in particular carbon particles do not accumulate at grain boundaries during deformation. The theoretical mean distance between two precipitates can be estimated from the carbon content in the material and from the particle volume. Assuming theoretical densities of 4 and 2 for alumina and graphite respectively, the graphite weight content of 1.3 % can be converted into a volume content of 2.6 %. From HRTEM, the volume of precipitates is about 10^3 nm^3. Thus, for a cubic distribution, the mean distance

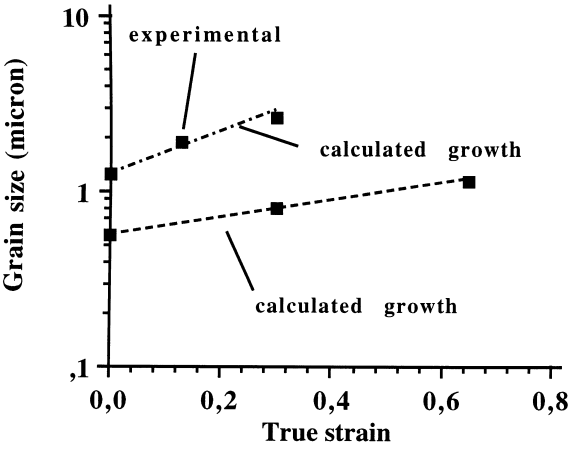

Fig. 8. Experimental data (square symbols) and calculated strain effect on grain growth at $T = 1400°C$.

Table 4
The different grain size exponent values (p) at $T = 1400°C$

Material atmosphere	UA vacuum	CA vacuum	CA Air
p (+/− 0.2)	1.6	2.35	2.13

between two precipitates is $(10^3/0.026)^{1/3}$, i.e. about 34 nm, in agreement with the distance estimated from TEM observations. The carbon precipitates have a slowing-down effect on the grain growth of UA material during its deformation. Even if the grain boundaries are not strongly pinned by the precipitates, their velocity perpendicular to grain boundary is greatly lowered by the high density of small and close obstacles. Let us compare the present strain rates and those that can be expected from single phase alumina polycrystals deformed in the same conditions (temperature, stress and grain size). The true strain rate obtained for CA material at $T=1400°C$ for $\sigma = 30$ MPa and $d=1.26$ μm was $\dot{\varepsilon}_0 = 7.10^{-5}$ s^{-1}. Considering a grain size $d=0.56$ μm the equivalent true strain rate is about $\dot{\varepsilon}_0 = 4.10^{-4}$ s^{-1} (using the average p value). The true strain rate of UA material at constant true stress $\sigma = 18$ MPa, $T=1400°C$ and $d=0.56$ μm is $\dot{\varepsilon} = 10^{-4}$ s^{-1}. At $\sigma = 30$ MPa its value would be $\dot{\varepsilon}_0 = 3.10^{-4}$ s^{-1} (using the average n value) which is very close to the first value. Hence the accommodation of the sliding by grain-boundary diffusion would not be altered by the presence of the precipitates.

The bonding of alumina/carbon interface shall not be too strong and the interface shall be able of diffusional transport as well as the alumina/alumina interface. This is required if the precipitates are not to affect the grain sliding during creep [14,15]. Indeed Niihara et al [15] reported about the creep inhibition of alumina/silicon carbide nanocomposites. The low diffusivity of the alumina/silicon carbide interface resulted in the creep inhibition and also in cavity formation. Here no intergranular cavity forms around graphite particles which strengthens the idea that the diffusivity of the alumina grain boundaries is not altered.

In terms of superplasticity the UA material deformation rates are comparable to that of the well-known superplastic zirconia in the studied stress and temperature ranges [9] (The zirconia deforms at a true strain rate of about $\dot{\varepsilon} = 3.10^{-4}$ s^{-1} at $\sigma = 30$ MPa and $T=1400°C$ for a grain size of about $d=0.5$ μm). Hence the initial small grain size associated with a reduced grain growth explains the improvement of deformation performances of the alumina.

4.4. Deformation and creep mechanisms

Deformation of such materials can result from intergranular mechanism involving grain shape changes similar to shape changes of the macroscopic specimen or from grain boundary sliding associated with minor grain shape changes.

In the present case the weak decrease in grain aspect ratio in strained materials supports the second hypothesis. Moreover, TEM observations showed that dislocation activity was not able to account for the achieved strains, which comforts the idea of the deformation mainly resulting from grain boundary sliding.

Concerning the accommodation mechanism even if cavities were observed after deformation in the CA material, they cannot explain such strains. Under these conditions it is likely that deformation is mainly diffusion accommodated for both materials. Besides thermomechanical parameters defined in relation (1) are consistent with this conclusion. However for a more precise understanding of deformation mechanisms those parameters must be now considered.

The activation energies in the range 500–580 $kJ.mol^{-1}$ are similar to the values reported in other studies [6–8] for pure and MgO-doped alumina. This range has usually been associated with Al cation diffusion processes [8]. However activation energies are not accurate enough to account unambiguously for the mechanisms responsible for deformation at the considered temperature, stress and grain size ranges.

According to the different descriptions of grain boundary sliding accommodation by diffusion, the grain exponent and the stress exponent have different values: $p=2$ and $n=1$ for bulk diffusion mechanism, $p=3$ and $n=1$ for grain boundary diffusion mechanism whereas $p=1$ and $n=2$ in the case of the interface reaction mechanism. However, when considering the simultaneous action of several deformation mechanisms, the experimental values of p and n are not so simple to analyse [17]. Generally it is admitted that the interface reaction mechanism is prevailing at small grain size or at low stress (less than 20 MPa) while the bulk and grain boundary diffusion are experienced at high stress (more than 80 MPa). The p and n values listed in Table 2 and Table 4 are not integers and support the fact that several mechanisms must act simultaneously in the stress, temperature and grain size ranges of the study. In this paper the limited investigated stress range corresponds to an intermediate stress domain. Hence it is not surprising that grain size or stress exponents are not integer. Nethertheless these exponents indicate a greater importance of the interface reaction mechanism for the UA material with respect to the CA one, an observation consistent with a finer grain size in the UA material. The difference of deformation mechanisms observed between the two materials shall be mainly related to the difference in grain sizes.

5. Conclusion

Microscopy observations of the alumina materials and testing showed the following

1. A finer microstructure is produced by hot-pressing when the material contains a small amount of carbon the distribution of which is fine and

homogeneous, both in the grain bulk and at the grain boundaries.
2. The deformation behaviour is greatly improved for the carbon-containing alumina (UA material). This is associated with the reduction of the grain growth during annealing or during high-temperature deformation.
3. The alumina diffusion-accommodated grain boundary sliding is not affected by the presence of graphite particles.
4. Considering the UA material, the large deformation capabilities are comparable to the ones currently obtained for superplastic zirconia.
5. The low flow stress associated with the high strain rate experienced by the UA material raises a good possibility of isothermal superplastic forging. This is the next step of the study.

References

[1] C. Carry, A. Mocellin, Structural superplasticity in single phase crystalline ceramics, Ceram. Int. 13 (1987) 89.
[2] F. Waka, T. Iga, T. Nagano, Effect of dispersions of ZrO_2 particles on creep of fine-grained Al_2O_3, J. Ceram. Soc. Jpn. 96 (1988) 1206.
[3] L.A. Xue, X. Wu, I.W. Chen, Superplastic alumina ceramics with grain growth inhibitors, J. Am. Ceram. Soc. 74 (1991) 842.
[4] X. Wu, I.W. Chen, Superplastic bulging of fine grained zirconia, J. Am. Ceram. Soc. 73 (1990) 746.
[5] L.A. Xue, I.W. Chen, Superplastic alumina at temperatures below 1300°C using charge compensating dopants, J. Am. Ceram. Soc. 79 (1996) 233.
[6] J.G. Wang, R. Raj, Mechanism of superplastic flow in a fine grained ceramic containing some liquid phase, J. Am. Ceram. Soc. 67 (1984) 399.
[7] K. Okada, Y.I. Yoshizawa, T. Sakuma, High temperature deformation in ZrO_2-Al_2O_3. in: S. Hori., M. Tokizane, N. Furushiro (Eds.), Superplasticity in Advanced Materials, The Jap. Soc. Res. on Superplasticity, 1991, p. 227.
[8] K.R. Venkatachari, R. Raj, Superplastic flow in fine-grained alumina, J. Am. Ceram. Soc. 69 (1986) 135.
[9] R. Duclos, J. Crampon, B. Amana, Structural and topological study of superplasticity in zirconia polycrystals, Acta Metall. Mat. 37 (1989) 877.
[10] H. Le Roux, An electron diffraction analysis of turbostratic graphite incemented carbides, Acta Metall. 33 (1985) 309.
[11] T.G. Nieh, J. Wadsworth, Dynamic grain growth during superplastic deformation of yttria-stabilized tetragonal zirconia polycrystals, J. Am. Ceram. Soc. 72 (1989) 1469.
[12] Y. I. Yoshizawa, & T. Sakuma, The strain-enhanced grain growth in tetragonal zirconia polycrystal during superplastic deformation, in: S. Hori., M. Tokizane, N. Furushiro (Eds.), Superplasticity in Advanced Materials, The Jap. Soc. Res. on Superplasticity, 1991, p. 251.
[13] D.S. Wilkinson, C.H. Caceres, On the mechanism of strain-enhanced grain growth during superplastic deformation, Acta Metall. 32 (1984) 1335.
[14] R. Raj, M.F. Ashby, Grain boundary sliding and diffusional creep, Metall. Trans. 2 (1971) 1113.
[15] T. Hirano, A. Nakahira, K. Niihara, Particle/matrix interface and its role in creep inhibition in alumina/silicon carbide nanocomposites, J. Am. Ceram. Soc. 79 (1996) 33.
[16] L. Clarisse, R. Baddi, A. Bataille, J. Crampon, R. Duclos, J. Vicens, Superplastic deformation mechanisms during creep of alumina-zirconia composites, Acta. Mater. 45 (1997) 3843.
[17] L. Clarisse, R. Baddi, J. Crampon, R. Duclos, Effect of duplex structure on the determination of the grain size exponent in zirconia polycrystals, J. Mater. Sci. Lett. 16 (1997) 71.